Progress In Electromagnetics Research, Vol. 127, 173–188, 2012

A NOVEL MULTILAYER DUAL-MODE SUBSTRATE INTEGRATED WAVEGUIDE COMPLEMENTARY FILTER WITH CIRCULAR AND ELLIPTIC CAVITIES (SICC AND SIEC)

Z.-G. Zhang*, Y. Fan, Y.-J. Cheng, and Y.-H. Zhang

Fundamental Science on Extreme High Frequency Key Laboratory, University of Electronic Science and Technology of China, Chengdu 611731, China

Abstract—A multilayer dual-mode complementary filter is developed based on substrate integrated circular and elliptic cavity (SICC and SIEC) in this paper. The filter is constructed with two different kinds of cavities, and each cavity supports two degenerate modes, which can be generated and controlled by the coupling aperture and slot located between layers. Detailed design process is introduced to synthesize an X-band dual-mode complementary filter. It not only has good performance, but also reduces the circuit size much more. Moreover, Sharp transition characteristic both in the lower and upper sidebands demonstrates high selectivity of the filter. Good agreement is obtained between the simulated and measured results of the proposed structure.

1. INTRODUCTION

Modern wireless communication systems are developed gradually towards higher integration and operating frequency band. As a matter of fact, compact microwave filters with high performance are required in many communication applications. So, substrate integrated waveguides (SIW) have been proposed [1–6] and applied to develop many high-quality components [13–19]. Furthermore, the SIW provides a promising solution to low cost and low profile, while good performance is maintained. Conventional SIW filters are based on rectangular cavities [1–3]. In [1], the SIW bandpass filters with improved stopband performance were presented for satellite ground

Received 7 February 2012, Accepted 6 April 2012, Scheduled 12 April 2012

* Corresponding author: Zhi-Gang Zhang (freeman_scu@yahoo.com.cn).

terminal. A compact SIW filter with defected ground structure (DGS) was proposed in [2]. Besides, the substrate integrated circular cavity (SICC) and elliptic cavity (SIEC) are good choices in the design of good performance filters [4–9]. They not only have the same attractiveness as classical SIW filters, but also present higher quality factor and lower loss. In [4], a new topology of coupling between SICCs was proposed to achieve particular filtering functions. In [8], a planar diplexer was developed based on dual-mode SICCs.

However, the SIW technology faces a new problem, i.e., the circuit size. Thus, the dual-mode technology [8–18] has been introduced in the design of SIW filter to meet the requirements in size reduction. A dual-mode SIW cavity can support two degenerate modes within one resonant unite, which not only reduces the circuit size more than half but also adds the design flexibility. On the other hand, the multilayer technology has become important, and is also another efficient way to achieve compact circuits. Therefore, the dual-mode and multilayer techniques can be employed together to achieve more compact SIW circuits. In [5], a fourth-order multilayer cross-coupled circular cavity filter was proposed by use of one slot introduced to suppress the spurious mode. In [9], a Ka-band 4-pole band pass filter was proposed using dual-mode SICCs, and the four layers circuit demonstrated an insertion loss of 2.95 dB and the stop-band rejection below 25 dB. To achieve better performance, in our previous works [13], a multilayer dual-mode filter was developed based on the SICCs. But, it can be found only one sideband of the filter is steep. Interestingly, a SIEC filter exhibits quite different characteristic compared with a SICC. Two transmission zeros (TZs) are located in the lower side response of the elliptic cavity. Accordingly, the SICC and SIEC techniques can be combined together to achieve multilayer complementary filter with higher performance.

In this paper, the complementary dual mode SICC and SIEC are firstly introduced in the multilayer SIW circuits, and a compact multilayer dual-mode filter with low loss, elliptic response and good performance has been achieved. The positions of coupling aperture and slot relative to the major axis of the SIEC can be adjusted to generate two modes. Meanwhile, it is possible to control the bandwidth and the rejection level by adjusting the parameters of the arc-shaped slot. The proposed structure is not only very compact, but also has lower insertion loss (1.65 dB), high selectivity and stop-band rejection. Moreover, it can be found that both the lower and the upper side response of the filter are very steep.

2. FILTER ANALYSIS AND DESIGN

2.1. Multilayer Dual-mode Complementary Filter Based on SICC and SIEC

As shown in Figure 1, there are two substrate layers. The input and output ports are distributed in the first and second layers, respectively. Two kinds of dual-mode cavity resonators are coupled through arc-shaped coupling slot in metal layer 2.

In these figures, α is the angle between the coupling slot and input/output port, R the radius of the SICC, R_a and R_b the semi-major and semi-minor axis of SIEC, respectively, W_C and W_S the widths of the coupling aperture and slot respectively, θ the central angle of the coupling slot, θ_2 the angle between the major axis of SIEC and output SIW, and W_g the width of SIWs.

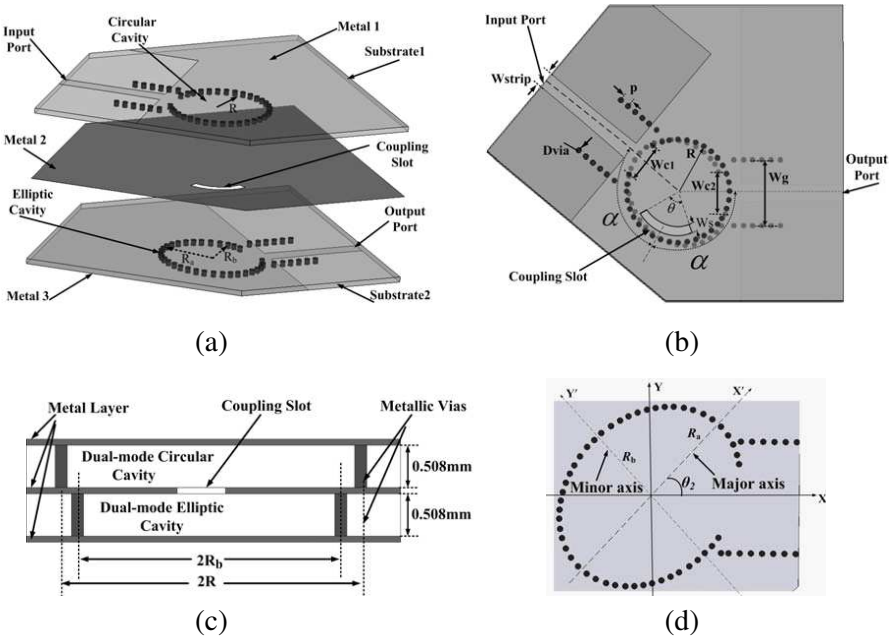

Figure 1. Proposed dual-mode SICC and SIEC filter with two layers. (a) Anatomy view. (b) Top view. (c) Side view. (d) Orientation of SIEC.

2.2. Dual Mode SICC and SIEC Principle

As is well known, the dual-mode phenomenon exists in many cavities including the SICC and SIEC. By adjusting the positions of coupling slots, the dual-mode character can be generated. Compared to the traditional rectangular cavity, the SICC and SIEC are more suitable to be used as dual-mode cavities due to their smooth inner surfaces. In a SICC, the degenerate modes are two orthogonal modes: the horizontal TM_{110} mode and the vertical TM_{110} mode. The resonant frequency of mode for circular cavity with solid wall can be calculated by [21].

$$f_{mnp} = \begin{cases} \frac{c}{2\pi\sqrt{\mu_r\varepsilon_r}}\sqrt{\left(\frac{\mu'_{mn}}{R}\right)^2 + \left(\frac{p\pi}{\Delta h}\right)^2} & TE_{mnp} \\ \frac{c}{2\pi\sqrt{\mu_r\varepsilon_r}}\sqrt{\left(\frac{\mu_{mn}}{R}\right)^2 + \left(\frac{p\pi}{\Delta h}\right)^2} & TM_{mnp} \end{cases} \tag{1}$$

where μ_r and ε_r are relative permeability and permittivity of the filling material, μ_{mn} and μ'_{mn} the nth roots of mth Bessel function of the first kind and its derivative, R the radius of circular cavity, Δh the height of the of circular cavity, and c the speed of light in free space. For $m > 0$, each m represents a pair of degenerate TM and TE modes ($\cos m\varphi$ or $\sin m\varphi$ variation). In circular cavity, TM_{110}, the second order mode, is selected as the working mode. Different directions represent different TM_{110} modes. μ_{mn} is 3.832 for the TM_{110} mode. Therefore, the corresponding resonant frequency of TM_{110} mode is:

$$f_{110} = \frac{c}{2\pi\sqrt{\mu_r\varepsilon_r}} \cdot \frac{3.832}{R} = \frac{0.61c}{R\sqrt{\mu_r\varepsilon_r}}, \tag{2}$$

Then, the radius of the SICC can be obtained:

$$R = \frac{0.61c}{f_{110}\sqrt{\mu_r\varepsilon_r}}. \tag{3}$$

However, in a SIEC, the two TM modes are not degenerated and have different resonant frequencies. They are denoted by TM_{cmnp} and TM_{smnp} modes, respectively. The resonant frequency for elliptic cavity with solid wall can be calculated by [6, 7]:

$$f_{mnp} = \frac{c \cdot \sqrt{q_{mnp}}}{R_a\pi e\sqrt{\mu_r\varepsilon_r}} = \frac{c}{\pi\sqrt{\mu_r\varepsilon_r}} \cdot \frac{\sqrt{q_{mnp}}}{\sqrt{R_a^2 - R_b^2}}, \tag{4}$$

$$\begin{aligned} &Ce_m(\xi_o, q) = 0, \quad \text{for } TM_{cm} \text{ mode} \\ &Se_m(\xi_o, q) = 0, \quad \text{for } TM_{sm} \text{ mode} \\ &Ce'_m(\xi_o, q) = 0, \quad \text{for } TE_{cm} \text{ mode} \\ &Se'_m(\xi_o, q) = 0, \quad \text{for } TE_{sm} \text{ mode.} \end{aligned} \tag{5}$$

where R_a and e are the semi-major axis and ellipticity of the SIEC, $\cosh \xi_o = 1/e$. R_b is the semi-minor axis. The parameter q is related to the resonant frequency, and there are a series of q values satisfying above Equations (5). To avoid ambiguity, a third subscript n, corresponding to the nth parametric root, is required in the mode designation, q_{mnp} is the nth parametric zero of the modified Mathieu functions of the first kind of the order m or their derivatives. Because of Mathieu functions' complicated calculation process, it is not very convenient to compute the parameters of a dual mode SIEC from Formula (4). Accordingly, the corresponding resonant frequency of quasi TM_{110} also can be computed by following approximate formula:

$$f_{c110} = \frac{c}{2\pi\sqrt{\mu_r\varepsilon_r}} \cdot \frac{1}{R_a} \cdot \sqrt{\frac{120\left(5 + 2(R_b/R_a)^2\right)\left(3 + (R_b/R_a)^2\right)}{101 + 80\left(R_b/R_a\right)^2 + 17(R_b/R_a)^4}}. \quad (6)$$

The resonant frequencies between the simulated results and obtained from (6) are compared as shown in Table 1. Due to a good agreement between the simulated and calculated results, it is concluded that the approximate formula can be used to determine the initial parameters of a dual-mode SIEC. Next, the solid wall is replaced by metallic vias to form SICC and SIEC under the guideline of [4, 5] and [20]. For the smaller ellipticity e, the resonant frequencies of TM_{c110} and TM_{s110} modes are approximately equal. Consequently, using formula (3) and (6) the initial dimensions of the cavities are determined for a desired resonant frequency.

Figures 2 and 3 show electrical fields of TM_{110} and quasi TM_{110} modes within the SICC and SIEC, respectively. Obviously, they are two orthogonal modes, which co-exist in the same cavity. The fields of the modes are distributed in different directions ($\cos\varphi$ or $\sin\varphi$ variation). The two degenerate modes in the SICC can be easily excited by setting the angle α between 100 and 130 degrees. Besides, the

Table 1. Resonance frequencies obtained from the simulation and the formula (6).

	R_a (mm), R_b (mm)	R (mm)	ε_r	Simulation (GHz)	Calculation (GHz)	Error (%)
1	13.3, 10.7	12	2.2	10.023	10.046	+0.26
2	13.6, 10.7	12.2	2.2	9.901	9.831	−0.55
3	13.5, 10.56	11.9	2.55	9.321	9.262	−0.64
4	5.026, 4.37	4.78	2.2	26.555	26.520	−0.13
5	13.4, 10.6	12.2	2.2	9.936	9.976	+0.40

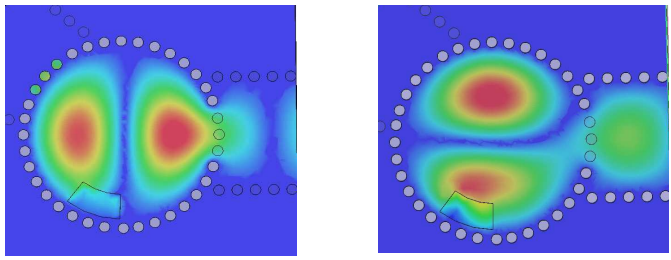

(a) (b)

Figure 2. The E-field distribution of the degenerate TM_{110} modes in SICC. (a) Vertical mode. (b) Horizontal mode.

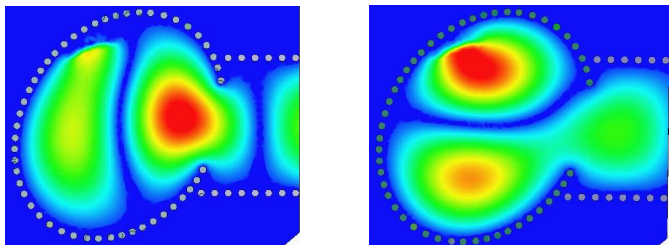

(a) (b)

Figure 3. The E-field distribution of the quasi TM_{110} modes in SIEC. (a) Vertical mode. (b) Horizontal mode.

TM_{c110} and TM_{s110} modes within the SIEC contribute to TZs located at lower sideband and are engaged in passband forming.

2.3. Coupling Slot

As shown in Figure 4, two poles and three TZs are found in the response of a dual-mode complementary filter. Two poles below the zero Z_{1up} are denoted as P_1 and P_2, respectively, which can be used to control the bandwidth. The first and second zeros near the passband are denoted as Z_{1d} and Z_{1up} respectively.

Being so close to the passband, zero Z_{1d} and Z_{1up} are both very helpful to realize a steeper side response. The space between the zero and pole decides the rolloff slope in the transition band. The coupling slot size determines the position of the first zero and then sets the slope of the side response. Figures 5 and 6 illustrate variations of poles, zeros with the coupling slot sizes W_S and θ changed.

The distance between the zero Z_{1d} and pole P_1 is increased as the coupling slot size W_S or θ increased, but the frequency of P_1, Z_{2up} is decreased evidently. Meanwhile, a small change occurs in the frequency

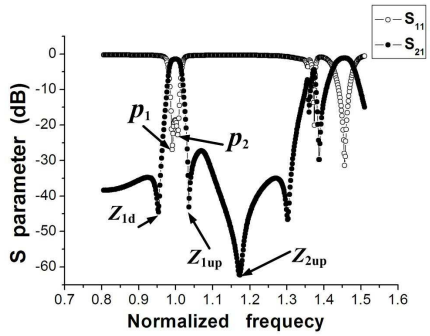

Figure 4. Response of dual-mode complementary filter.

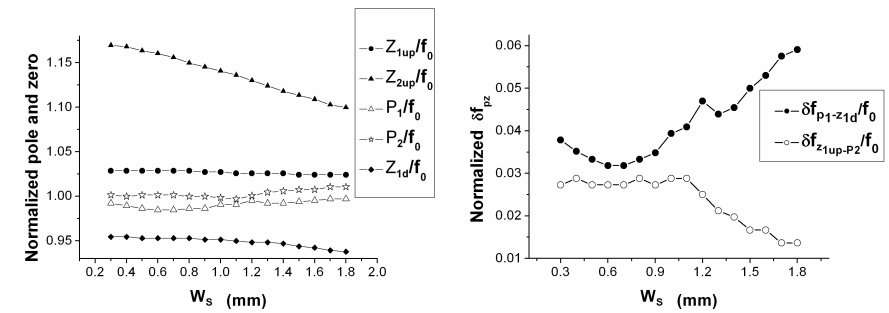

Figure 5. Variation of poles, zero and the distance between pole and zero with W_S, where, $\delta f_{p1-z1d} = f_{p1} - f_{p2}$, $\delta f_{z1up-P2} = f_{z1up} - f_{p2}$, $\theta = 36^\circ$, f_0 is the eigenfrequency of TM_{110} mode.

of P_2 and Z_{1up}. As shown in Table 2, the coupling is increased when the slot size increased. Then, it is possible to control the bandwidth and the rejection level. When the slot size is changed, the positions of P_1, P_2 and Z_{1d}, Z_{2up} are also influence in operating frequency. As observed in Figures 5 and 6, the distance between the zero Z_{1d} and pole P_1 decreases evidently with the width of coupling slots W_S or θ decreased. As a result, the steeper rolloff slope and narrower bandwidth are obtained.

Figure 7 shows the relationship between zero Z_{2up} and α in the complementary cavities. Obviously, Z_{2up} is independent of eigenmodes. The distance between Z_{2up} and the center frequency f_0 are increased with the angle α. To suppress the undesirable spur, the angle α should be adjusted carefully to assure Z_{2up} over the spur. Generally, smaller α or θ corresponds to narrower bandwidth and steeper rolloff slope in transition band, and vice versa.

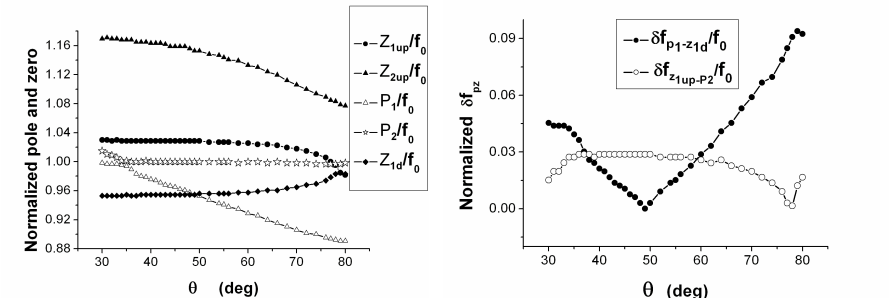

Figure 6. Variation of poles, zero and the distance between pole and zero with θ, where, $\delta f_{p1-z1d} = f_{p1} - f_{p2}$, $\delta f_{z1up-P2} = f_{z1up} - f_{p2}$. $W_S = 0.4\,\text{mm}$, f_0 is the eigenfrequency of TM_{110} mode.

Table 2. Relative bandwidth change with θ and W_S.

θ (deg)	δ_{p1-z1d}/f_0	$\Delta f/f_0$ (%)	W_s (mm)	δ_{p1-z1d}/f_0	$\Delta f/f_0$ (%)
30	0.045	3	0.3	0.039	2.9
35	0.042	3.3	0.4	0.037	3.3
38	0.029	3.7	0.6	0.032	3.75
40	0.027	4.39	0.7	0.033	3.9
60	0.028	4.5	0.8	0.035	4.1

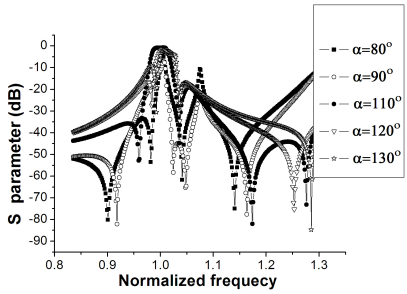

Figure 7. Relation between zero Z_{2up} and α in complementary cavity (SICC/SIEC).

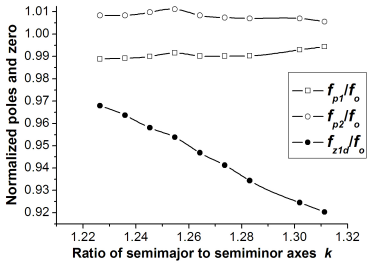

Figure 8. Relations of poles P_1, P_2, and zero Z_{1d} to k. Here, $k = R_a/R_b$, $W_{c1}/R = 0.66$, $W_{c2}/R = 0.81$, $R_a = 10.6\,\text{mm}$, $\alpha = 110°$.

As observed in Table 3, angle α also affects the bandwidth of the complementary filter. A large value of α should be chosen for a broadband filter, while a small α may be proper for a narrowband filter. From the above discussion, α determines the second zero Z_{2up},

Table 3. $\Delta f/f_0$ change with α.

W_{c1}/R	W_{c2}/R	α (deg)	$\Delta f/f_0$ (%)
0.65	0.785	110	3.5
0.65	0.785	120	3.8
0.65	0.785	130	4.3

Table 4. Relative bandwidth change with the parameters k and e.

k	e	W_{c1}/R	W_{c2}/R	α (deg)	$\Delta f/f_0$ (%)
1.216	0.569	0.66	0.81	110	2.37
1.235	0.587	0.66	0.81	110	3.21
1.241	0.592	0.66	0.81	110	3.45
1.265	0.612	0.66	0.81	110	3.66
1.311	0.646	0.66	0.81	110	3.80

which is in the stop band and close to the adjacent TM_{210} mode. The proper value of α is between 100 and 130 degrees.

The relationship of the poles and zero with respect to the parameter k is shown in Figure 8. It can be seen that poles are almost kept constant, but Z_{1d} is linearly decreased as k increased. The space between P_1 and Z_{1d} is enlarged. Similarly, the ellipticity e determines the position of the first zero Z_{1d}.

As illustrated in Table 4, the parameters k and e are also important factors affecting the bandwidth. So, a large value of k or e should be chosen for a broadband filter, and vice versa.

2.4. External Feeding Structure

The tapered microstrip transitions are proposed to feed the SICC and SIEC as the input/output ports. As shown in Figure 1, the waveguide located in input/output port can be used to suppress some undesirable response spur and improve the stop band characteristic.

As observed in Figure 9 and Table 5, the bandwidth and rolloff slope in the transition band are affected by W_{c1}/R and W_{c2}/R for a given angle α. In general, smaller W_{c1}/R and W_{c2}/R lead to narrower bandwidth and steeper rolloff slope in the transition band.

Moreover, for a given angle α, the proper parameters W_{c1}/R and W_{c2}/R are limited in a relatively narrow interval. Beyond the limit, either the dual-mode phenomenon disappears or the response performance worsens.

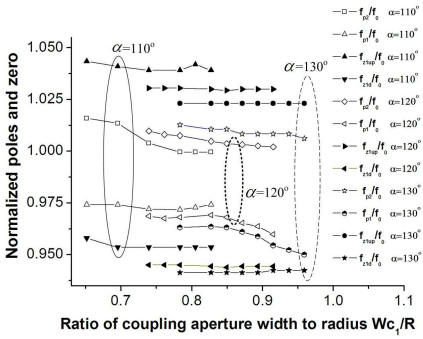

Figure 9. Variation of poles and zeros Z_{1d}, Z_{1up} with respect to W_{c1}/R. Here, f_0 is the eigenfrequency of TM_{110} mode, R is the radius of the circular cavity, $W_{c2}/R = 0.78$.

Table 5. $\Delta f/f_0$ change with W_{c1}/R and W_{c2}/R.

W_{c1}/R	W_{c2}/R	α (deg)	$\Delta f/f_0$ (%)	W_{c1}/R	W_{c2}/R	α (deg)	$\Delta f/f_0$ (%)
0.63	0.72	110	3.1	0.7	0.79	130	3.8
0.68	0.78	110	3.37	0.78	0.88	130	4.1
0.82	0.87	110	3.6	0.85	0.96	130	4.5

2.5. Design Example

In our design, the center frequency and bandwidth of the filter are 10 GHz and 350 MHz, respectively. The used substrate is Rogers 5880 with relative permittivity (ε_r) of 2.2 and height of 0.508 mm. Here, the SICC and SIEC operate at TM_{110} and quasi TM_{110} modes, respectively. In the present design, the first step is to decide the dimensions of SICC and SIEC cavities. By using the Formulas (2) and (3), the initial values of radius of SICC cavities (R) should be 12.3 mm. According to Formula (6) and Table 4, the semi-major (R_a) and semi-minor (R_b) axes of the SIEC should be 13.3 mm and 10.7 mm.

The second step is to calculate the coupling coefficients and external quality factor. Two TZs are located at upper side of the passband, and the other is located at the lower side of the passband. The coupling scheme of the proposed dual-mode complementary filter is presented in Figure 10. Resonators 1, 2 and 3, 4 represent two orthogonal modes, respectively.

Then, external quality factor Q of such a filter meeting these requirements can be extracted by the certain technique of optimization

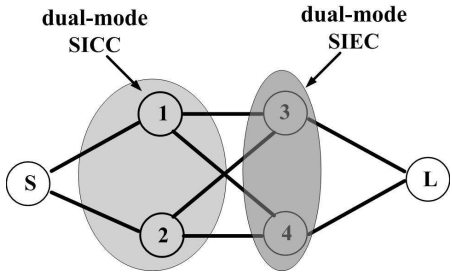

Figure 10. Coupling scheme of fourth-order dual-mode filter (gray areas show dual-mode cavities).

adopted in [22], and given by

$$Q_{ei} = Q_{eo} = 41.93 \tag{7}$$

As shown in Figures 1(a) and (b), the coupling between SICC and SIEC is realized by introducing an arc slot in the common wall between them. The coupling strength between the two cavities depends on all of the geometrical parameters of the filter, which is described by the coupling coefficient calculated by [23]:

$$M_{i,j} = \pm \frac{f_e^2 - f_m^2}{f_e^2 + f_m^2} \tag{8}$$

where f_e and f_m are the resonant frequencies of two coupling cavities corresponding to its symmetrical plane replaced by an electric wall and a magnetic wall, respectively. From Figure 10 we find that the source is coupled to both modes with: M_{S1} and M_{S2}. M_{3L} and M_{4L} denote the coupling between load and each resonator, respectively.

The third step is to realize the coupling coefficients and external quality factor. The external quality factor is controlled by the width of the coupling aperture (W_{c1}, W_{c2}) and given directly by (7). The coupling slot is located close to the maximum magnetic fields of the SICC/SIEC cavities. From above discussion, the initial parameters of slot and cavities will be determined as flowing steps:

(a). Based on above discussion, the angle α is the key factor to realize the two TM modes in multilayer SICCs and SIECs. The dual-mode character is easily excited by setting the angle α between 100 and 130 degrees. To achieve better stop band rejection, the distance between Z_{2up} and the center frequency f_0 can be decreased by selecting the smaller α. According to Table 3, the proper value of α is 110°.

(b). The parameters of the arc-shape coupling slot: W_S, θ. The coupling slot size determines the bandwidth and the positions of the

zeros. According to Figures 5, 6 and Table 2, the initial geometrical parameters of slot are determined. One can choose the width of the coupling slot with $W_S = 0.6\,\text{mm}$, the central angle $\theta = 36^\circ$.

(c). The bandwidth and rolloff slope in the transition band are affected by W_{C1}/R and W_{C2}/R. As shown in Figure 9 and Table 5, the widths of the coupling apertures are determined as $W_{C1}/R = 0.7$, $W_{C2}/R = 0.8$. By adjusting the angle θ_2 in Figure 1(d), we can control the relative strengths of the TM_{c110} and TM_{s110} modes in a SIEC. Furthermore, when $\theta_2 = 30^\circ$, 45°, and 55°, the resonant frequencies of TM_{c110} and TM_{s110} modes are approximately equal and can coexist in the same passband of a narrow band filter. So, they contribute to TZ located at lower side band. To achieve better response performance, one can choose the orientation angle with $\theta_2 = 55^\circ$.

For a given angle $\alpha = 110^\circ$, the proper parameters are limited in a relatively narrow interval. According to Table 5 and the specifications, the value ranges for W_{C1}/R and W_{C2}/R are from 0.65 to 0.8 and 0.75 to 0.85, respectively. Similarly, as observed in Table 2, the value ranges for W_S, θ are from 0.4 to 0.8 and 35° to 39° respectively. According to above considerations, the final optimal dimensions of the proposed filter can be easily determined.

3. EXPERIMENT RESULTS

Based on the above-discussed theories, the multilayer dual-mode complementary filter is designed and fabricated with PCB process. Figure 11 shows the photograph of the fabricated dual-mode filter.

After optimization implemented by Ansoft HFSS, the geometry parameters of the proposed filter are listed in Table 6. All the transition tapers from the SIWs to microstrips are the same with a length of 8 mm and widths of 3 and 1.58 mm at two ends. As shown in Figure 12, the fabricated filter has a center frequency of 10.03 GHz with

Table 6. Parameters of the fabricated filter.

D_{via} (mm)	0.8	W_{strip} (mm)	1.58
p (mm)	1.5	W_g (mm)	15
ε_r	2.2	W_{c1} (mm)	8.2
W_S (mm)	0.5	h (mm)	0.508
α (deg)	110	R (mm)	12.2
θ (deg)	37	W_{c2} (mm)	9.7
R_a (mm)	13.4	R_b (mm)	10.6

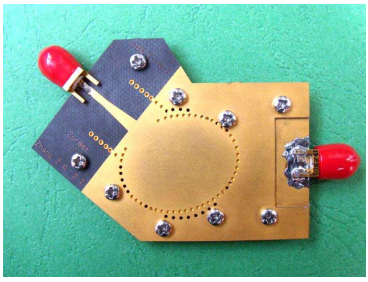

Figure 11. Photograph of the fabricated filter.

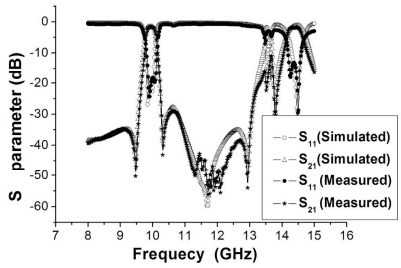

Figure 12. Simulated and measured results of the dual-mode complementary filter.

a bandwidth of 345.3 MHz. The maximum return loss is 19.5 dB within the passband and the insertion loss is about 1.65 dB. It is demonstrated that measured results agree very well with simulated ones except for a little frequency offset. Three TZs are located at 9.47, 10.35, and 11.3 GHz, respectively. Its stop band is from 7.2 to 9.5 GHz and 11.2 to 12.8 GHz with the rejection more than 35 dB.

Compared with the multilayer dual-mode filter based on double SICCs, the proposed structure has lower selectivity (still higher than [9]). Its main reason is that a SICC contributes only to the TZs located at upper side band, and a SIEC is helpful to realize the TZs located at lower side. However, the proposed structure not only has double steep transition bands, lower insertion loss, but also has TZs located at both upper and lower side band. To achieve higher selectivity, an additional SICC or SIEC can be introduced in the proposed structure without increasing the circuit size.

4. CONCLUSION

A novel multilayer dual-mode complementary filter has been designed, fabricated, and measured in this paper. The complementary SICC and SIEC are firstly introduced in the 3-D multilayer SIW circuits, and a compact dual-mode filter with low loss, elliptic response and good performance has been achieved. The bandwidth and restraint outside the band can be controlled by adjusting the parameters of the coupling aperture and arc-shaped slot. The measured maximum return loss is 19.5 dB over pass band while the insertion loss is about 1.65 dB. Good agreement is obtained between the simulated and measured results of the proposed structure. This structure is very compact and well suited for the microwave and millimeter wave applications.

ACKNOWLEDGMENT

This work is supported in part by the National Natural Science Foundation of China (NSFC) under grant 61001028 and in part by Research Fund for the Doctoral Program of Higher Education of China (RFDP) under grant 20100185110014, and in part by the Fundamental Research Funds for the Central Universities under grant ZYGX2010J019.

REFERENCES

1. Chen, X. P. and K. Wu, "Substrate integrated waveguide filter with improved stopband performance for satellite ground terminal," *IEEE Trans. Microw. Theory Tech.*, Vol. 57, No. 3, 674–683, Mar. 2009.
2. Shen, W., W. Y. Yin, and X. W. Sun, "Compact substrate integrated waveguide (SIW) filter with defected ground structure," *IEEE Microw. Wirel. Compon. Lett.*, Vol. 21, No. 2, 83–85, Feb. 2011.
3. Deslandes, D. and K. Wu, "Substrate integrated waveguide dual-mode filters for broadband wireless systems," *RAWCON'03, Proceedings*, 385–388, Aug. 2003.
4. Potelon, B., J. F. Favennec, E. Rius, and J. C. Bohorquez, "Design of a substrate integrated waveguide (SIW) filter using a novel topology of coupling," *IEEE Microw. Wirel. Compon. Lett.*, Vol. 18, No. 9, 596–598, Sep. 2008.
5. Wei, Q.-F., Z.-F. Li, and L.-S. Wu, "Compact cross-coupled circular cavity filters using multilayer substrate integrated waveguide," *Electron. Lett.*, Vol. 45, No. 6, Mar. 12, 2009.
6. Zhang, S. J. and Y. C. Shen, "Eigenmode sequence for an elliptical waveguide with arbitrary ellipticity," *IEEE Trans. Microw. Theory Tech.*, Vol. 43, No. 1, 227–230, Jan. 1995.
7. Accatino, L., G. Bertin, and M. Mongiardo, "Elliptical cavity resonators for dual-mode narrow-band filters," *IEEE Trans. Microw. Theory Tech.*, Vol. 45, No. 12, 2393–2401, Dec. 1997.
8. Tang, H. J., W. Hong, J.-X. Chen, G.-Q. Luo, and K. Wu, "Development of millimeter-wave planar diplexers based on complementary characters of dual-mode substrate integrated waveguide filters with circular and elliptic cavities," *IEEE Trans. Microw. Theory Tech.*, Vol. 55, No. 4, 776–781, Apr. 2007.
9. Ahn, K. and I. Yom, "A ka-band multilayer LTCC 4-pole bandpass filter using dual-mode cavity resonators," *IEEE*

MTT-S International Microwave Symposium Digest, 1235–1238, Jun. 2008.

10. Hu, G., C. Liu, L. Yan, K. Huang, and W. Menzel, "Novel dual mode substrate integrated waveguide band-pass filters," *Journal of Electromagnetic Waves and Applications*, Vol. 24, Nos. 11–12, 1662–1672, 2010.
11. Wang, J.-P., L. Wang, Y.-X. Guo, Y. X. Wang, and D.-G. Fang, "Miniaturized dual-mode bandpass filter with controllable harmonic response for dual-band applications," *Journal of Electromagnetic Waves and Applications*, Vol. 23, Nos. 11–12, 1525–1533, 2009.
12. Zhao, L.-P., X.-W. Dai, Z.-X. Chen, and C.-H. Liang, "Novel design of dual-mode dual-band bandpass filter with triangular resonators," *Progress In Electromagnetics Research*, Vol. 77, 417–424, 2007.
13. Zhang, Z. G., Y. Fan, Y. J. Cheng, and Y.-H. Zhang, "A compact multilayer dual-mode substrate integrated circular cavity (SICC) filter for X-band application," *Progress In Electromagnetics Research*, Vol. 122, 453–465, 2012.
14. Wei, C. L., B.-F. Jia, Z.-J. Zhu, and M. Tang, "Design of different selectivity dual-mode filters with E-shaped resonator," *Progress In Electromagnetics Research*, Vol. 116, 517–532, 2011.
15. Chen, C.-H., C.-S. Shih, T.-S. Horng, and S.-M. Wu, "Very miniature dual-band and dual-mode bandpass filter designs on an integrated passive device chip," *Progress In Electromagnetics Research*, Vol. 119, 461–476, 2011.
16. Cheng, Y. J., W. Hong, K. Wu, and Y. Fan, "Millimeter-wave substrate integrated waveguide long slot leaky-wave antennas and two-dimensional multibeam applications," *IEEE Transactions on Antennas and Propagation*, Vol. 59, No. 1, 40–47, Jan. 2011.
17. Hu, J. P., G. H. Li, H. P. Hu, and H. Zang, "A new wideband triple-band filter using SIR," *Journal of Electromagnetic Waves and Applications*, Vol. 25, No. 16, 2287–2295, 2011.
18. Hu, G., Y. Chen, X. Zhao, K. Huang, and C. Liu, "Novel high selective bandpass filters incorporated with quasi-lumped impedandce inverters," *Journal of Electromagnetic Waves and Applications*, Vol. 25, No. 10, 1382–1390, 2011.
19. Liu, B., F. Wei, H. Zhang, X. Shi, and H. Lin, "A tunable bandpass filter with switchable bandwidth," *Journal of Electromagnetic Waves and Applications*, Vol. 25, Nos. 2–3, 223–232, 2011.

20. Xu, F. and K. Wu, "Guided-Wave and leakage characteristics of substrate integrated waveguide," *IEEE Microw. Theory Tech.*, Vol. 53, No. 1, 66–70, Jan. 2005.
21. Pozar, D. M., *Microwave Engineering*, 2nd edition, Wiley, New York, 1998.
22. Cameron, R. J., "General coupling matrix synthesis methods for chebyshev filtering functions," *IEEE Trans. Microw. Theory Tech.*, Vol. 47, No. 4, 433–442, Apr. 1999.
23. Hong, J. S. and M. J. Lancaster, *Microstrip Filters for RF/Microwave Applications*, Chapter 8, 235–272, Wiley, New York, USA, 2001.